Sensitive Injury Detection in the Cervical Spine Using Acoustic Emission and Continuous Wavelet Transform

Jay K. Shridharani, Brian R. Bigler, Courtney A. Cox, Maria A. Ortiz-Paparoni, Cameron R. 'Dale' Bass

Abstract

Assessing the initiation of failure is critical to understanding the progression of spinal injuries and to developing injury criteria. These incipient injuries are being assessed more frequently using acoustic emissions. However, the signals tend to be chaotic especially under high-rate loading where simply the presence of acoustic emissions does not necessarily indicate injury. Therefore, this paper presents a technique to interrogate the acoustic emission signals to determine when cortical bone failure occurs. Isolated cortical bone specimens were loaded at 10 mm/min to failure and the resulting acoustic emissions had wideband response with peaks from 20 to 900 kHz, with the dominant peak being 59.6 ± 21.9 kHz (mean ± standard deviation). Whole cervical spines were then loaded at fast rate (1.2 m/s) to cause injury. A continuous wavelet transform using a Morlet mother wavelet showed the 59.6 kHz frequency component entered the time domain at many points in time, which could be calculated using the described algorithm. The first point was determined to indicate the initiation of failure due to its low amplitude, and the following two points suggested larger failure. This work presents a necessary set of tools for effectively utilising acoustic emissions in biological material testing.

Keywords acoustic emission, bone failure, frequency characterisation, wavelet transform

I. INTRODUCTION

Spinal injuries cause large societal expenses due to the long-term debilitating pain and widespread morbidity [1-4]. The gross failure mechanics of the spine have been studied extensively, primarily focusing on the static and dynamic loads that result in extensive mechanical damage [5-13]. However, the criteria for the initiation of failure are not well established primarily because they are difficult to assess. Although localised injuries (e.g. cortical shell disruption, localised trabeculae failure, etc.)[14-17] likely do not have the long-term consequences associated with major injuries such as burst fractures, wedge fractures, etc. [18,19], minor injuries are hypothesised to be precursors to major injuries [9,20], especially for repetitive exposure. Therefore, understanding the failure mechanics of minor injuries is important in understanding the initiation of major injuries.

Current techniques for detecting failure in biological tissues often rely on observing discontinuities or inflection points in a material's force-displacement curve (Fig. 1). While these characteristics suggest material failure, they may also result from the underlying material geometry (e.g. cervical spine buckling)[5,21,22]. Acoustic emissions can be used to sensitively assess material failure during crack propagation [23]. They are regularly used to detect the initiation of damage at the material level (e.g. concrete, metals, glass, ceramics, composites) to more complex multi-material structures (e.g. bridges, buildings, pressure vessels). This technique works on the principle that acoustic waves are emitted during the release of energy at material failure independent of the extent of failure [23]. These techniques are commonly used in biological material testing to assess material failure when its detection is difficult [24-31]. However, most of these studies assume that any acoustic emission is a direct result of material failure. In reality, acoustic emissions can result from sources that do not indicate failure, such as test apparatus vibration. An accurate characterisation of the acoustic emissions from bony failure is needed to confidently assess bone failure/injury.

J. K. Shridharani is a PhD candidate in Biomedical Engineering at Duke University in Durham, NC, USA (tel: +1 919-660-8272, jay.shridharani@duke.edu). B. R. Bigler, C. A. Cox, and M. A. Ortiz-Paparoni are PhD candidates in Biomedical Engineering at Duke University in Durham, NC, USA. C. R. 'Dale' Bass is an Associate Research Professor in Biomedical Engineering at Duke University in Durham, NC; USA, and the primary advisor to these four students.

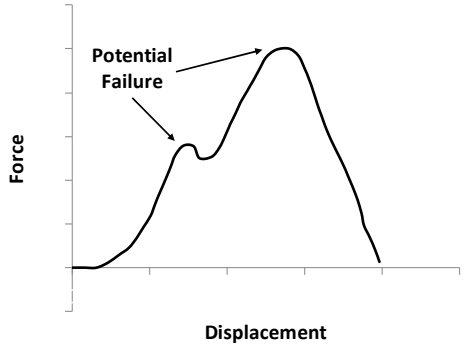

Fig. 1. Example of a force displacement loading curve being used to identify material failure.

Separating the frequencies of interest during highly energetic dynamic loading situations, in which the acoustic emission signals are superimposed with specimen/test apparatus vibration, is critical in assessing the timing of injury. There are many methods to determine the time-frequency response of signals. Short Time Fourier Transforms (STFT) divide a signal into individual, discrete, overlapping time series. A windowing function is used to prevent spectral leakage and the power spectrum is calculated over each time segment. This provides an indication of when specific frequencies enter the time domain; however, there is a tradeoff between time and frequency resolution vs available computational memory. Also, both the time and frequency resolution are generally lower than that compared to a continuous wavelet transform (CWT).

Continuous wavelet transforms were developed to address the issues with STFT and provide greater time and frequency resolution. Instead of calculating the frequency spectrum of discrete time histories, CWTs are a convolution of a wave packet sweeping through time. Information on different frequency regions is obtained by changing the shape of the *mother* wavelet. By squeezing and stretching the wavelet in time, information is gained on the high and low frequency components respectively. This technique provides much greater time and frequency resolution. However, the ability to see changes in the frequency response can be dependent on mother wavelet selection. Although continuous wavelet transforms offer potential improvements in time and frequency resolution, the tradeoff between time and frequency resolution still exists, and cannot be avoided.

II. METHODS

The methodology in this study has been organised into two parts. The first part determines the acoustic emission (AE) response from bony injuries while the second uses this determined response to pinpoint the timing of failure in a whole cervical spine failure test. This study was performed in accordance with the research protocol approved by the Duke University Institutional Review Board, NC, USA.

Cortical Bone Acoustic Characterisation

Three cortical bone specimens were excised from the anterior region of human thoracic vertebral bodies (T3-T4) and cleaned of all soft tissue, including the periosteum, using an osteotome. Although the primary objective is to characterize the acoustic emission response of cervical vertebral body bone, thoracic specimens were used as surrogates under the assumption that the AE response will be similar to that of cervical vertebral bone. Donor age, weight, stature, and specimen dimensions can be found in (Table I). Trabecular bone was removed to direct the load path through the cortical bone. Two to four piezoelectric acoustic sensors (Model S9225, Physical Acoustic Corporation, Princeton Junction, NJ 08550, USA) were adhered to the cortical bone using cyanoacrylate glue and used to measure acoustic emissions during testing. The acoustic sensors were sampled at 125 MHz at 14 to 15-bit resolution using a digital oscilloscope (Model 5444B, Pico Technology, Tyler, TX, 75702, USA) to obtain high resolution timing of the AE with adequate bandwidth. The trigger level was set to 5 mV above the steady state noise to avoid missing any AEs.

TABLE I
DONOR ANTHROPOMETRY FOR CORTICAL BONE SPECIMENS

Specimen Number (#)	Age (years)	Mass (kg)	Height (cm)	Dimensions W x H (mm x mm)
1	77	68	178	22.69 x 19.7
2	66	94	185	24.16 x 18.77
3	77	74	180	17.51 x 22.08

A custom test apparatus (Fig. 2) was built to apply compressive loading at low rates. The displacement was measured using a string potentiometer (Model LX-PA, UniMeasure, Corvallis, OR, 97333, USA) and the force was measured using a single axis 220 N (50 lb) load cell (Model 31, Honeywell Sensing and Control, Golden Valley, MN 55422, USA). The vertical guide rails and cups were made out of polycarbonate to ensure no metal was in the same field of view as the specimen during CT imaging allowing the capture of CT images without metal artifacts.

The specimen was secured in the polycarbonate cups using a fast-curing urethane resin (#891, Golden West Mfg., Inc., Grass Valley, CA 95945, USA). Screws were not used in the fixation for two reasons: (1) due to the risk of causing premature failures at the fixation points that may influence the AE response and (2) to prevent causing artifacts in CT images. Instead, the ends of the specimen were placed in the urethane as it cured providing a custom fit and support for the specimen. Compression was applied at low loading rate (10 mm/min) until an AE was observed, at which point the data acquisition system sent a 5 V transistor-transistor logic (TTL) signal to the stepper motor controller seizing the movement and preventing further loading. This was done to isolate a single acoustic emission and a single injury endpoint. Micro computed tomography (microCT) images were then acquired at 20 µm nominal resolution to confirm injury. If a positive confirmation of injury was not found, the specimen was reloaded and this procedure was repeated until positive confirmation was attained.

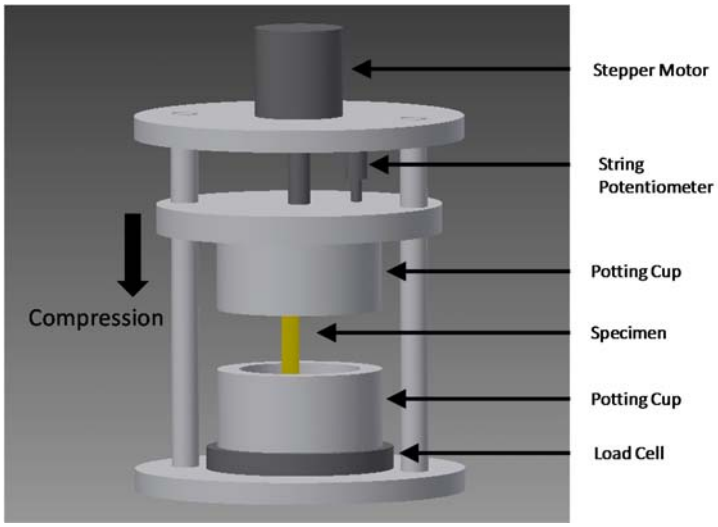

Fig. 2. Custom test apparatus designed to apply compressive loading without causing artifacts in CT images. No metal is in the same field of view as the specimen: the stepper motor, string potentiometer, and load cell are the only parts containing metal.

Signal analysis was performed in Python (v3.4.3) using the Numpy (v1.10.4), Scipy (v0.17.0), and Machine Learning Python (v3.5.0) packages. The spectral content of each acoustic emission was analysed using a Welch power spectrum density estimate. The Welch estimate was selected due to its lower sensitivity to noise compared to a periodogram or a power spectrum density. The spectral response peaks were selected and compiled together from all of the tests. The peaks of each sensor with the highest power were used to characterise the spectral response of the cortical bone failure.

Detecting Bone Failure in Dynamic Loading Testing

Three whole osteoligamentous cervical spine specimens were dissected from whole body specimens. Only enough musculature, skin, fat, and periosteum were removed from the anterior region of the specimens to allow sensor placement. The specimens were frozen fresh and maintained in a -20 °C freezer prior to preparation. Donor anthropometry can be found in (Table II). The basilar skull and T1 were included leaving the atlanto-occipital through C7-T1 joints intact and these were used as platforms to provide loading to the specimen. Wood screws were attached to the basilar skull and T1 to provide additional adhesion to the potting materials and polymethylmethacrylate (PMMA) was wrapped around these screws to distribute the stress. These ends were then potted in aluminum cups using a fast-curing urethane resin (#891, Golden West Mfg., Inc., Grass Valley, CA 95945, USA) placing the specimen in a pre-flexed posture by angling the Frankfort plane at 25° from horizontal, the T1-OC angle at 10° ± 5° from vertical, and the Cobb angle at 15° ± 5°, and. The specimen was placed in a servohydraulic materials testing machine by rigidly attaching the superior pot to the frame and the inferior pot to the piston.

TABLE II
DONOR ANTHROPOMETRY FOR WHOLE CERVICAL SPINE SPECIMENS

Specimen Number (#)	Age (years)	Mass (kg)	Height (cm)
1	61	64	168
2	75	72	183
3	66	94	185

A total of 10 miniature acoustic sensors (Model S9225, Physical Acoustic Corporation, Princeton Junction, NJ 08550, USA) were adhered to the cortical bone of each specimen lateral to the anterior longitudinal ligament using cyanoacrylate glue and two hydrophones (Model TC-4013, Teledyne RESON A/S, Slangerup, Denmark) were placed against the pedicles using a flexible tie. These locations are summarised in Table III and a diagram of the setup is shown in Fig. 3. The acoustic sensors have sufficient response from 100 kHz to 2 MHz and the hydrophones from 1 Hz to 170 kHz with greater sensitivity than the acoustic sensors. These sensors were used together to provide a wideband characterisation of the acoustic response. The acoustic sensors are small (3.6 mm x 2.4 mm) compared to the hydrophones (9.5 mm x 25 mm) which allowed the placement of an array of sensors. Failure was expected to occur in bending near C4, so more sensors were placed on this vertebral body in order to capture the event with minimal risk of instrumentation errors. In additional to the acoustic sensors, a 6-axis load cell (Model MC5-6-5000, Advanced Mechanical Technology, Inc., Watertown, MA 02472, USA) was used to measure the applied force and a linear variable differential transformer (LVDT) (Model DC-ED-10000, Measurement Specialties, Hampton, VA 23666, USA) was used to measure the piston displacement.

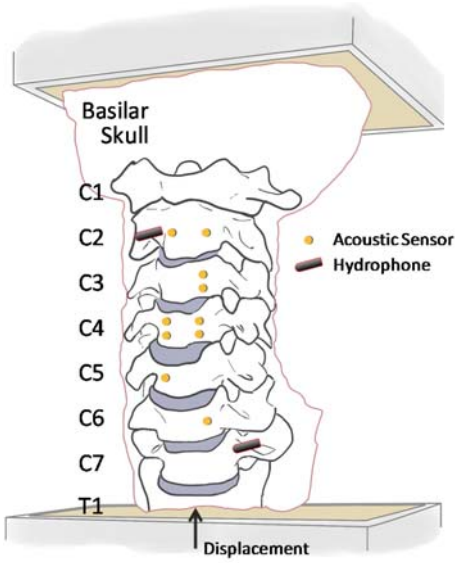

Fig. 3. Acoustic sensors and hydrophones were instrumented at various locations along the specimen. Note that the hydrophones were placed against the pedicles posterior to the transverse processes.

The piston was moved upward in displacement control to apply a compressive ramp-hold displacement at as high of a loading rate as possible (nominally 1.2 m/s) to a maximum displacement known to cause injury based on previous experience (nominally 5-10% strain). This loading rate and profile was chosen to unquestionably create injury and produce a chaotic, dynamic environment consisting of test apparatus vibration that would complicate the injury detection using the acoustic sensors.

Injuries were identified through necropsies by carefully dissecting the muscle and skin to expose interest regions. Then visual assessment of the specimen was performed to detect soft tissue damage (e.g. ligament ruptures, inter vertebral disc bulging). Range of motion for each joint was assessed in anterior-posterior bending, lateral bending, and torsion. Joints were then disarticulated by cutting through the middle of the intervertebral disc and all connecting ligaments. The remaining soft tissue was cleaned and bone structures (i.e. vertebral body, spinous, transverse, and articular processes, facets, lamina, and pedicles) were inspected for fractures.

The acoustic signals were analysed using a CWT with a Morlet mother wavelet providing a map of when different frequency content entered the time domain. The Morlet wavelet follows the form

$$\psi(\eta) = \pi^{-1/4} e^{i\omega_o \eta} e^{-\eta^2/2} \quad (1)$$

where ω_o is the nondimensional frequency chosen to be 2 and η is the nondimensional time chosen to be 0.05. The continuous wavelet transform was calculated as the convolution of the discretely sampled x_n with the scaled and translated version of $\psi(\eta)$[32]:

$$W_n(s) = \sum_{n'}^{N-1} x_{n'} \psi^* \left[\frac{(n'-n)\delta t}{s}\right] \quad (2)$$

The Morlet wavelet was chosen as the mother wavelet because it is similar in shape to acoustic emissions. The frequencies with the maximum power at each point in time were selected and compared to the frequencies of interest determined in the previous testing phase. The timing of bony failure was calculated based on when this frequency entered the time domain. An autoregressive (AR) Akaike information criterion (AIC) function [33] was used to calculate this time of arrival:

$$AIC(k) = k \log\big(var(x[0,k])\big) + (N-k+1) \log\big(var(x[k+1,N])\big) \quad (3)$$

where x is the amplitude at the chosen frequency through time, k is the time index in the x array of length N, and var is the variance.

TABLE III
LOCATION OF ACOUSTIC SENSORS

Vertebral Body	Model S9225		Model TC-4013 Hydrophone	
	# of Sensors	Sensor Location	# of Sensors	Sensor Location
C2	2	Left (1x), Right (1x)	1	Left Pedicle
C3	2	Left	-	-
C4	4	Left (2x), Right (2x)	-	-
C5	1	Right	-	-
C6	1	Left	-	-
C7	-	-	1	Right Pedicle

III. RESULTS

Cortical Bone Acoustic Characterisation

Cortical bone failure was produced in all specimens (Fig. 4) and typically consisted of long crack formation. Individual, isolated acoustic emissions were measured and generally detected by each sensor adhered to the

specimen (Fig 5a). Each specimen was loaded at least twice before a positive identification of injury could be obtained from the microCT images. The acoustic signals show very small differences in their time of arrivals (<4 µs) and initial high frequency oscillation followed by a lower frequency long-term response (Fig 5b). The Welch power spectrum density estimate (Fig. 6) shows wideband frequency content with distinct peaks. Spectral peaks were found from 20 kHz to 900 kHz. The peak with the maximum power is summarised in Table IV for all specimens and sensors with a mean frequency of 59.6 ± 21.9 kHz (mean ± standard deviation).

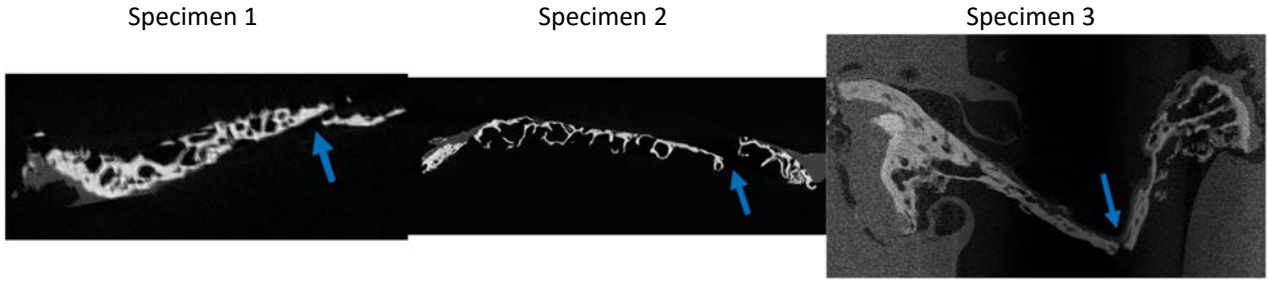

Fig. 4. MicroCT images at 20 µm resolution of the cortical bone failures in three specimens. Images show some trabecular bone was not fully removed prior to testing but cortical bone failed in each test.

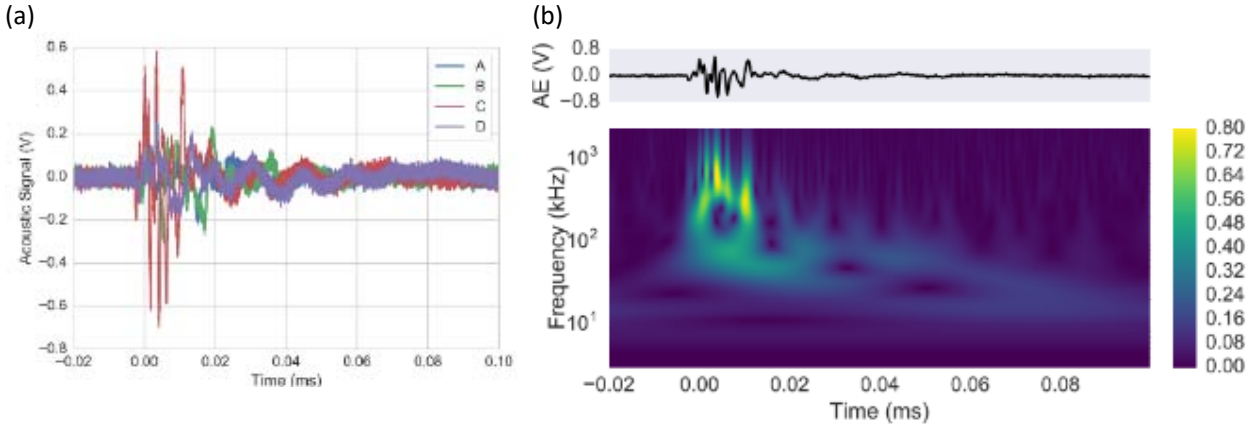

Fig 5. (a) Time history of an acoustic emission from cortical bone failure in specimen 1 and (b) CWT of sensor 3 showing acoustic emission frequency entering the time domain at distinct points in time.

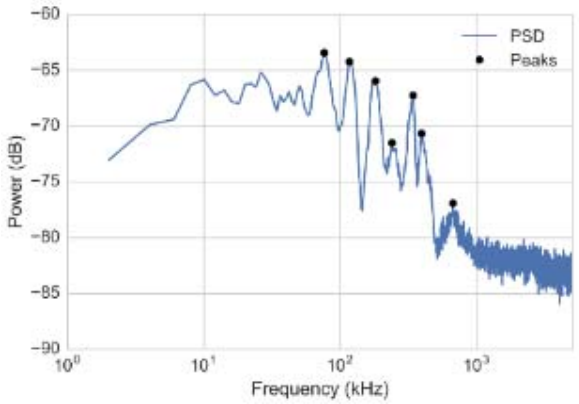

Fig. 6. Welch power spectrum density estimate of an AE from cortical bone failure in specimen 1 measured by sensor 2. Notice the wideband response from 58 to 925 kHz and the distinct peaks.

TABLE IV
SPECTRAL PEAKS FROM CORTICAL BONE FAILURE

Specimen (#)	Sensor (#)	Frequency (kHz)	Power (dB)
1	1	36	-63.5
	2	76	-61.9
	3	64	-59.2
	4	72	-58.7
2	1	42	-64.2
	2	86	-49.3
	3	42	-55.7
3	1	96	-57.3
	2	40	-37.7
	3	42	-40.2

*The AE response consisted of dominant spectral components at 59.6 ± 21.9 kHz (mean ± standard deviation)

Detecting Bone Failure in Dynamic Loading Testing

Three whole cervical spines were loaded until failure at fast loading rate (1.2 m/s). Multiple AEs were detected before and near the peak force and displacement (Fig. 8a-c). Small amplitude AEs occurred between 30-35 ms prior to the larger AEs near the peak force. The CWT (Fig. 8d-e) shows wideband spectral content from 5 kHz to 400 kHz. The algorithm calculated the 59.6 kHz frequency content entered the time domain at three distinct points in time for Specimen 1 and 2, and at seven points in time for Specimen 3 and were determined to indicate cortical bone failure at these times. The necropsies revealed bony and endplate injuries in each specimen (Table V, **Error! Reference source not found.**).

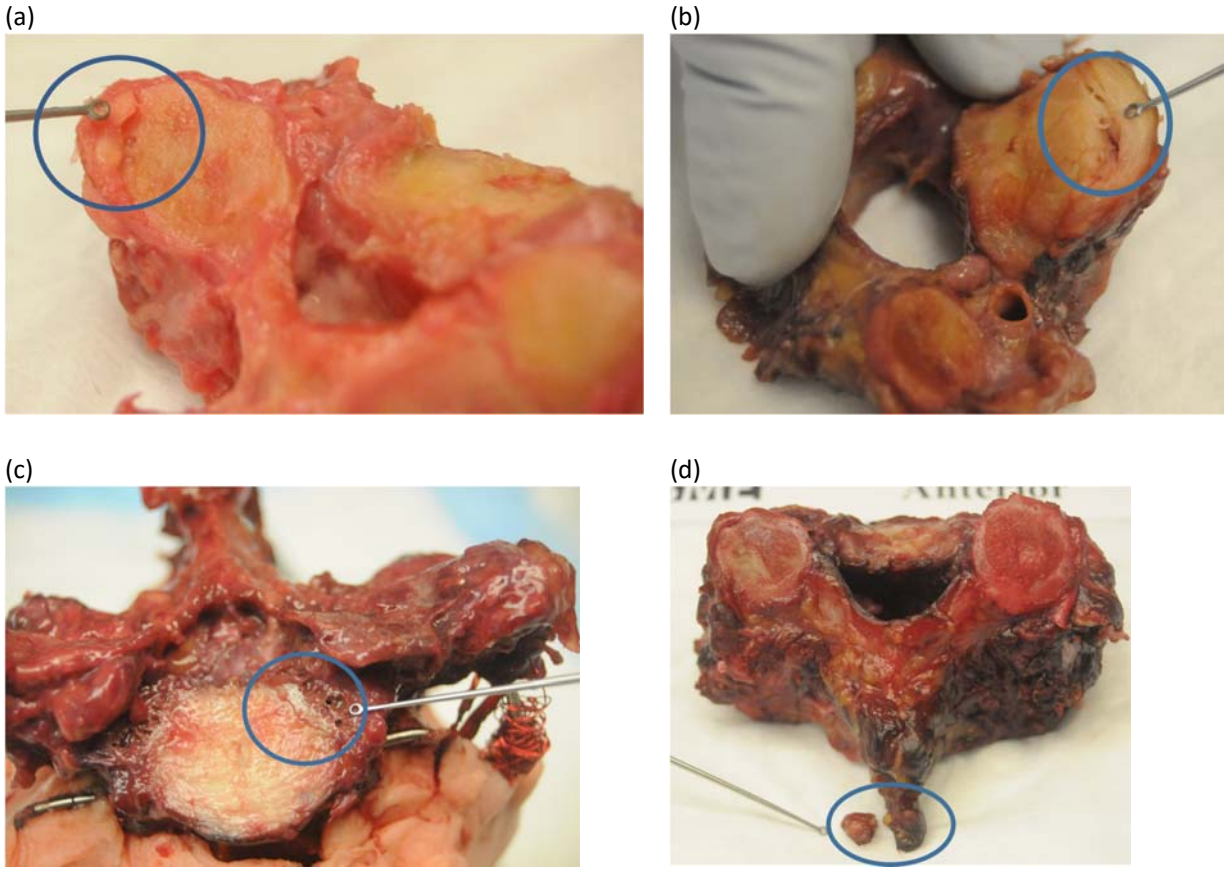

Fig. 7. Following the dynamic loading test, necropsy revealed failures at (a) Specimen 1 C5 superior left facet, (b) Specimen 2 C3 inferior endplate, (c) Specimen 3 T1 superior left uncinated process, and (d) Specimen 3 C6 spinous process.

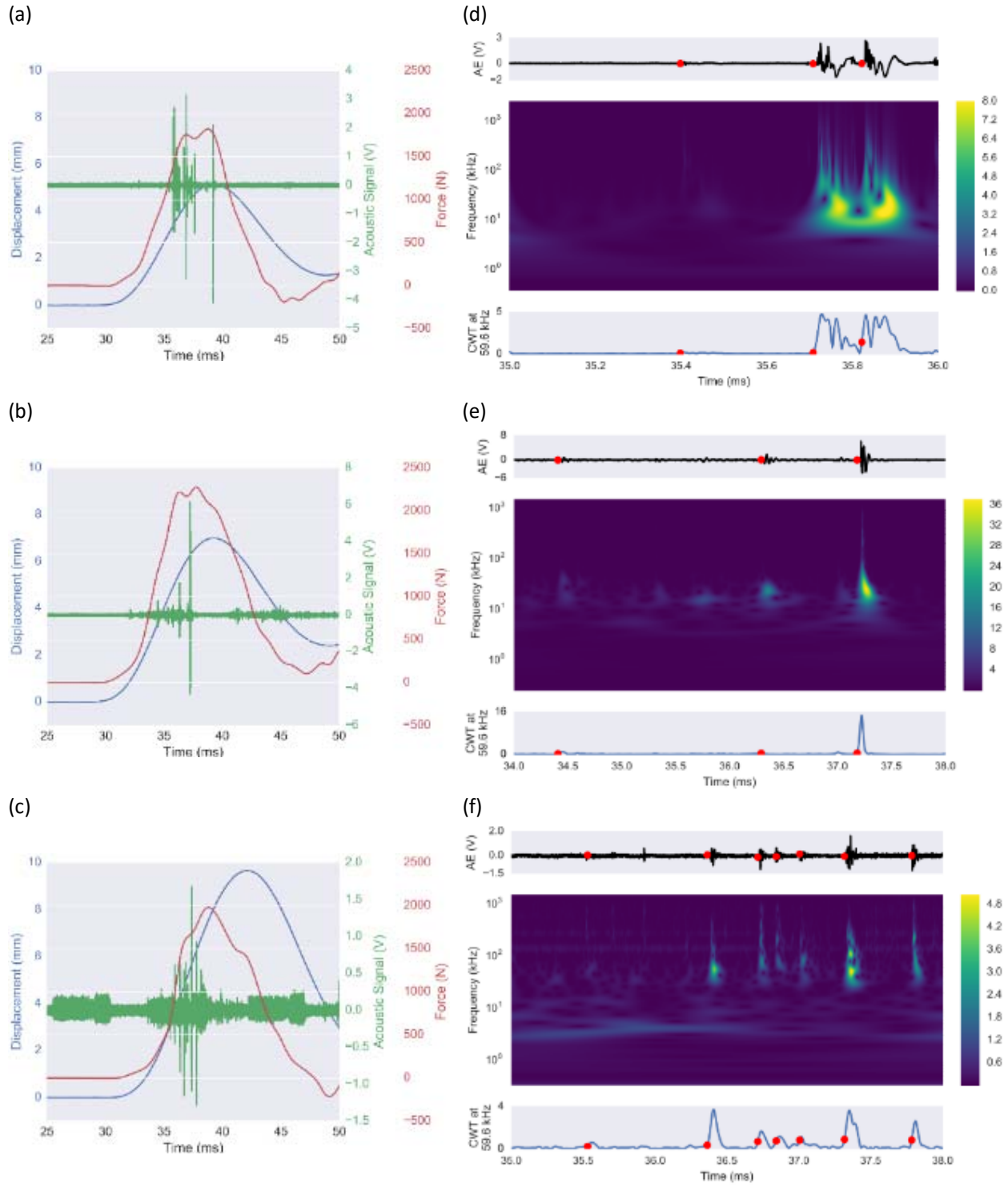

Fig. 8. (A-C) Time history of the acoustic signal, applied force, and applied displacement for all three specimens (D-E) Acoustic emission signal (top), CWT (middle), and CWT at 59.6 kHz (bottom) for an AE during a whole cervical spine failure test. The red dots show the calculated time of arrivals for the 59.6 kHz frequency component.

TABLE V
INJURIES FOUND IN NECROPSY

Specimen Number (#)	Injury
1	C5 superior left facet Fx
2	C3 inferior endplate Fx
3	C6 spinous process Fx T1 left uncinated process Fx

IV. DISCUSSION

Cortical Bone Acoustic Characterisation

Few studies have investigated the frequency response of AEs from biological tissue material failure [26-28,31]. Typically, the induced injury has extensive damage consisting of cortical bone and trabecular failure causing the measured acoustic signal to include the superposition of multiple AEs complicating the characterization of the spectral response. Additionally, the tests in these studies are dynamic and often at high rate causing degradation of the signals from vibrational modes in the specimen or test apparatus. In the current study, loading was applied at a quasi-static low rate to limit the influence of non-injury related acoustic signals. The loading was immediately stopped at the first sign of acoustic signals after which the injury was confirmed with high resolution microCT images. This provided confidence that the acoustic emission was a direct result of the material failure with limited influence from external factors.

The spectral peak at 59.6 kHz found in this study is similar to those found in previous studies [26,27], however additional higher frequency peaks up to 925 kHz were detected. This is likely because higher frequencies attenuate more quickly in bone [34]. The signals likely attenuated less in our study because the specimens were smaller and the sensors were placed close to the injury site. Furthermore, most of the trabecular bone was removed from the specimens in this studies, therefore strengthening the hypothesis that the observed spectral peaks are a direct result of cortical bone failure since trabecular bone can act as a filter attenuating acoustic signals [35]. The whole cervical spine test did not show these high frequency components further suggesting they are due to the close proximity of the sensors to the injury site.

One limitation of this study is that the S9225 sensors used in this study have less sensitivity to frequencies in the 0-300 kHz range than the 300-1900 kHz range, limiting the ability to detect lower frequency components. This is typically done by design to filter out the non-failure related signals, but this frequency band is important to detecting cortical bone failure and likely for soft tissue failure. The frequencies detected in this range likely have higher power than what was observed, which increases the confidence that the frequencies reported in Table IV are representative of cortical bone failure.

Detecting Bone Failure in Dynamic Loading Testing

The primary difficulty in the analysis of acoustic emissions in dynamic testing is determining which components of the signal are indicative of material failure and determining when the failure occurs. A simple Fourier transform or power spectrum density does a sufficient job of providing the frequency content of the signal, but it is unable to elucidate when frequencies occur or how frequencies change throughout time. Spectrograms have been used to combat this issue [31], but their fundamental technique is limited in temporal and spectral resolution. Wavelet transforms provide a much better representation of the signal but those too are not without limitations. Primarily, the analysis is met with a constant resistance from Heisenberg's uncertainty principle. More specifically, additional spectral resolution cannot be attained without sacrificing temporal resolution. The results can often differ based on the selection of the mother wavelet, the shape parameters, and the selection of scales. Therefore, a balance must be struck to obtain information on when specific material failure occurs. The analysis in this paper focuses on gaining temporal resolution by first determining the frequencies of interest from isolated cortical bone testing and then performing a CWT to determine when these frequencies occur.

The proposed technique illustrates the ability to assess when specific frequencies enter the time domain.

Cortical bone failure is considered to occur at the points in time when the 59.6 kHz frequency component initiates. In each specimen, low-amplitude acoustic emission(s) were observed during the initial loading period suggesting the initiation of failure followed by two larger amplitude AEs, which may suggest the propagation of the initial injury or larger injuries occurring at another location. Although these AEs can be visually identified (Fig. 8a-c), this technique determines the timing of the failure for closely spaced AEs without being influenced by the low frequency, slowly-dissipating signal components. The time histories in Specimen 2 and 3 would allude to additional fractures at 35.3 and 35.7 ms respectively, however the lack of power at 59.6 kHz suggests this is not the case.

This technique is limited in that it assumes the frequency band from cortical bone failure will always include 59.6 kHz, however this frequency band may be attenuated causing the response to be dominated by lower frequency components. We recommend using an array of sensors distributed over the specimen and analyze the response from the sensor with the earliest time of arrival to limit the influence of this assumption. Additionally, this criterion is based on the maximum power of variable spectral peaks with wideband responses. We believe some of this wideband response is due to the small size of our specimens as mentioned above and the larger frequency components would therefore rarely be observed in larger specimens. Using a single spectral peak as the criteria for all cortical bone failures is certainly questionable especially considering the range of spectral peaks (Table IV). However, we do not believe that a single (or multiple) optimal spectral peaks exists to describe cortical bone failure due to the confounding effects caused the distance between the fracture and the sensor, specimen composition, specimen age, etc. Instead, it is better to find a spectral peak that often exists within the band of frequencies associated with cortical bone failure. A methodology to dynamically assess the accuracy of the injury timing results presented earlier would be of great value to assess the validity of the 59.6 kHz frequency criteria.

An additional limitation is that the failure always occurs earlier in time than what this technique would suggest due to the time it takes the AE to travel from the failure location to the sensor. This leads to conservative estimates of the failure loads providing an additional factor of safety. Additionally, each mother and daughter wavelet do not encompass a single frequency but instead a band of frequencies. The frequency content of a specific scale was estimated based on the centre frequency at that scale. Therefore, slight error in amplitude at each frequency exists but likely has limited influence on calculated timing of failure.

V. CONCLUSIONS

This is the first study to extensively characterie the acoustic emission response from cortical bone and provide a technique to assess the timing of cortical bone failure in dynamic testing where multiple failures could occur and where acoustic signals may occur from non-failure events. Contrary to prior studies, cortical bone failure produces wideband AE signals whose dominant component is similar to previous literature. Knowing the frequency components for cortical bone failure and having a method of determining when these frequencies occur is imperative to understanding the progression of spinal injuries and to the development of failure criteria.

VI. ACKNOWLEDGEMENT

The authors would like to thank the Naval Air Systems Command (NAVAIR) and the U.S. Army Research, Development and Engineering Command (contract #N00024-13-D-6400) for providing funding for this work. The content included in this work does not necessarily reflect the position or policy of the U.S. government.

VII. REFERENCES

[1] Côté, P., Cassidy, J.D., and Carroll, L. The Saskatchewan Health and Back Pain Survey: The Prevalence of Neck Pain and Related Disability in Saskatchewan Adults. *Spine*, 1998. 23(15): p. 1689-1698

[2] Harrop, J.S., Sharan, A.D., Vaccaro, A.R., and Przybylski, G.J. The cause of neurologic deterioration after acute cervical spinal cord injury. *Spine*, 2001. 26(4): p. 340-346

[3] Sekhon, L.H.S. and Fehlings, M.G. Epidemiology, Demographics, and Pathophysiology of Acute Spinal Cord Injury. *Spine*, 2001. 26(24S): p. S2-S12

[4] Daffner, S.D., Hilibrand, A.S., et al. Impact of Neck and Arm Pain on Overall Health Status. *Spine*, 2003. 28(17): p. 2030-2035

[5] Nightingale, R.W., McElhaney, J.H., Richardson, W.J., and Myers, B.S. Dynamic responses of the head and

cervical spine to axial impact loading. *Journal of Biomechanics*, 1996. 29(3): p. 307-318
[6] Van Ee, C.A., Nightingale, R.W., et al. Tensile properties of the human muscular and ligamentous cervical spine. *Stapp car crash journal*, 2000. 44: p. 85-102
[7] Ito, S., Ivancic, P.C., Panjabi, M.M., and Cunningham, B.W. Soft Tissue Injury Threshold During Simulated Whiplash: A Biomechanical Investigation. *Spine*, 2004. 29(9): p. 979-987
[8] Ivancic, P.C., Pearson, A.M., Panjabi, M.M., and Ito, S. Injury of the anterior longitudinal ligament during whiplash simulation. *European Spine Journal*, 2004. 13(1): p. 61-68
[9] Bass, C.R., Lucas, S.R., et al. Failure Properties of Cervical Spinal Ligaments Under Fast Strain Rate Deformations. *Spine*, 2007. 32(1): p. E7-E13
[10]Nightingale, R.W., Carol Chancey, V., et al. Flexion and extension structural properties and strengths for male cervical spine segments. *Journal of Biomechanics*, 2007. 40(3): p. 535-542
[11]Stemper, B.D., Storvik, S.G., et al. A New PMHS Model for Lumbar Spine Injuries During Vertical Acceleration. *Journal of Biomechanical Engineering*, 2011. 133(8): p. 081002-081002
[12]Panjabi, M.M., Pearson, A.M., et al. Cervical Spine Ligament Injury during Simulated Frontal Impact. *Spine*, 2004. 29(21): p. 2395-2403
[13]Pearson, A.M., Panjabi, M.M., et al. Frontal Impact Causes Ligamentous Cervical Spine Injury. *Spine*, 2005. 30(16): p. 1852-1858
[14]Vernon-Roberts, B. and Pirie, C.J. Healing trabecular microfractures in the bodies of lumbar vertebrae. *Annals of the Rheumatic Diseases*, 1973. 32(5): p. 406-412
[15]Twomey, L. and Taylor, J. Whiplash Injury and Neck Sprain: A Review of Their Prevalence, Mechanisms, Risk Factors, and Pathology. 2005. 17(4): p. 285-300
[16]Lu, W.W., Luk, K.D.K., et al. Microfracture and Changes in Energy Absorption to Fracture of Young Vertebral Cancellous Bone Following Physiological Fatigue Loading. *Spine*, 2004. 29(11): p. 1196-1201
[17]Van Goethem, J.W., Ozsarlak, O., and Parizel, P.M. Cervical spine fractures and soft tissue injuries. *JBR-BTR*, 2003. 86(4): p. 230-234
[18]Silverman, S.L. Osteoporotic Vertebral FractureThe clinical consequences of vertebral compression fracture. *Bone*, 1992. 13: p. S27-S31
[19]Scane, A.C., Sutcliffe, A.M., and Francis, R.M. The sequelae of vertebral crush fractures in men. *Osteoporos Int*, 1994. 4(2): p. 89-92
[20]Brinckmann, P., Biggemann, M., and Hilweg, D. Fatigue fracture of human lumbar vertebrae. *Clinical Biomechanics*, 1988. 3: p. i-S23
[21]Nightingale, R.W., McElhaney, J.H., et al. The dynamic responses of the cervical spine: buckling, end conditions, and tolerance in compressive impacts. 1997, SAE Technical Paper.
[22]Panjabi, M.M., Cholewicki, J., et al. Critical load of the human cervical spine: an in vitro experimental study. *Clinical Biomechanics*, 1998. 13(1): p. 11-17
[23]Kohn, D.H. Acoustic Emission and Nondestructive Evaluation of Biomaterials and Tissues. *Critical Reviews in Biomedical Engineering*, 1995. 23(3-4): p. 221-306
[24]Aggelis, D., Paschos, N., et al. Rupture of anterior cruciate ligament monitored by acoustic emission. *The Journal of the Acoustical Society of America*, 2011. 129(6): p. EL217-EL222
[25]Paschos, N., Aggelis, D., et al. An Acoustic Emission Study for Monitoring Anterior Cruciate Ligament Failure Under Tension. *Experimental Mechanics*, 2012: p. 1-8
[26]Van Toen, C., Street, J., Oxland, T.R., and Cripton, P.A. Acoustic emission signals can discriminate between compressive bone fractures and tensile ligament injuries in the spine during dynamic loading. *Journal of Biomechanics*, 2012. 45(9): p. 1643-1649
[27]Funk, J., Bass, C., et al. Dynamic crack detection in the human tibia using acoustic emission. *Proceedings of Proceedings of the 28th International Workshop on Human Subjects for Biomechanical Research*, 2000.
[28]Funk, J.R., Khaewpong, N., et al. The Axial Injury Tolerance of the Human Foot/Ankle Complex and the Effect of Achilles Tension. *Journal of Biomechanical Engineering*, 2002. 124(6): p. 750-757
[29]Kent, R., Stacey, S., and Parenteau, C. Dynamic Pinch Tolerance of the Phalanges and Interphalangeal Joints. *Traffic Injury Prevention*, 2008. 9(1): p. 83-88
[30]Cormier, J., Manoogian, S., et al. The Tolerance of the Frontal Bone to Blunt Impact. *Journal of Biomechanical Engineering*, 2011. 133(2): p. 021004-021004
[31]Shridharani, J.K., Schmidt, A.L., et al. Dynamic Failure Localization in Spinal Specimens using Acoustic Emissions. *Proceedings of IRCOBI Conference Proceedings*, 2014.
[32]Torrence, C. and Compo, G.P. A practical guide to wavelet analysis. *Bulletin of the American Meteorological*

society, 1998. 79(1): p. 61-78
[33]Maeda, N. A method for reading and checking phase times in auto-processing system of seismic wave data. *Zisin= Jishin*, 1985. 38(3): p. 365-379
[34]Sasso, M., Haïat, G., Yamato, Y., Naili, S., and Matsukawa, M. Frequency Dependence of Ultrasonic Attenuation in Bovine Cortical Bone: An In Vitro Study. *Ultrasound in Medicine & Biology*, 2007. 33(12): p. 1933-1942
[35]Lin, W., Serra-Hsu, F., Chen, J., and Qin, Y.-X. Frequency Specific Ultrasound Attenuation Is Sensitive to Trabecular Bone Structure. *Ultrasound in medicine & biology*, 2012. 38(12): p. 2198-2207